Microsolvation of heavy halides

Chamorro, Yuly; Flórez, Edison; Maldonado, Alejandro; Aucar, Gustavo; Restrepo, Albeiro

Published in:
International Journal of Quantum Chemistry

DOI:
10.1002/qua.26571

Publication date:
2021

Received: 27 August 2020 | Revised: 31 October 2020 | Accepted: 5 November 2020

DOI: 10.1002/qua.26571

FULL PAPER

International Journal of Quantum Chemistry WILEY

Microsolvation of heavy halides

Yuly Chamorro[1,2] | Edison Flórez[3] | Alejandro Maldonado[4] | Gustavo Aucar[4] | Albeiro Restrepo[1]

[1]Instituto de Química, Facultad de Ciencias Exactas y Naturales, Universidad de Antioquia UdeA, Medellín, Colombia

[2]Van Swinderen Institute for Particle Physics and Gravity, Faculty of Science and Engineering, University of Groningen, Groningen, The Netherlands

[3]School of Natural and Computational Sciences, College of Sciences, Centre for Theoretical Chemistry and Physics, The New Zealand Institute for Advanced Study, Massey University Auckland, Auckland, New Zealand

[4]Departamento de Física, Facultad de Ciencias Exactas y Naturales, Universidad Nacional del Nordeste, Corrientes, Argentina

Correspondence
Albeiro Restrepo, Instituto de Química, Universidad de Antioquia, Medellín 050010, Colombia.
Email: albeiro.restrepo@udea.edu.co

Funding information
Cociencias, Grant/Award Number: 111571249844; Consejo Nacional de Investigaciones Científicas y Técnicas, Grant/Award Number: PIP112-201301-00361; Fondo para la Investigación Científica y Tecnológica, Grant/Award Number: PICT2016-2936; Universidad de Antioquia, Grant/Award Number: Estrategia para la sostenibilidad

Abstract

The fundamental question of how intermolecular interactions lead to the stabilization of heavy halides (Br^-, I^-, At^-) microsolvated with up to six explicit water molecules is addressed here. An exhaustive exploration of the potential energy surfaces using a random search algorithm followed by optimization of molecular geometries using pseudopotentials and at the full four component relativistic levels of theory, affords a good number of structures with high probabilities of occurrence, highlighting the important role of local minima to reproduce experimentally measured properties. Sequential hydration enthalpies for astatide are reported here for the first time in the scientific literature. Closed shell (ionic, long range) as well as intermediate character interactions (contributions from closed shell and covalent) are at play stabilizing the clusters. The ability of water molecules to either donate or to accept electron density dictates the nature and strength of the corresponding hydrogen bonds in solvation shells. Binding energies and molecular geometries are shown to be more sensitive to electron correlation than to relativistic effects.

KEYWORDS

heavy halides, intermolecular interactions, microsolvation, potential energy surfaces, relativistic effects

1 | INTRODUCTION

Br^-, I^-, the heavy halides, play an essential role in a number of physicochemical processes that take part in aqueous environments. A testament to the scientific interest in microsolvated heavy halides is the extensive literature devoted to the problem using both experimental [1–6] and computational approaches [7–18]. Just to illustrate the point, we hand pick a few relevant topics associated with microsolvation of these species: Br^-, I^- are major players in the global climate because they are part of aerosols commonly found in the stratosphere [19–23]. Heavy halides have also been identified as health hazards because, when they are found in drinking water sources, they react with disinfecting agents leading to cancer and birth defects related substances [24–26]. Astatine is considered a promising radiotherapy agent in nuclear medicine [27]. However, because ^{210}At, the most stable isotope has a lifetime of only 8.1 h, there is no spectroscopic data on its properties, nonetheless, there is no shortage of analytical [28–31] and computational [29, 30, 31, 32–36] studies. Most prominently, At^- has recently been detected in biological systems [28] and electromobility measurements have shown it to exist in aqueous media [28, 31]. It is also thought to be involved in radioactive labeling mechanisms [37].

In the context of this work, essential aspects of heavy halide research may be highlighted: (i) Potential energy surfaces (PES) for the microsolvation of heavy halides have not been exhaustively studied, thus, relevant structural features may have been overlooked. (ii) The reduced sampling of structural possibilities aside, those works have focused on the energetic and spectroscopic sides of the problem, leaving the important aspect of the nature of the intermolecular halide↔water interactions as well as the influence of the formal charge on the surrounding networks of hydrogen bonds, mostly unexplored. (iii) It is unfortunate that to the best of our knowledge, relativistic effects on the structures, energies, and bonding on the hydration of heavy halides have not been studied. (iv) Because of fast decay times, very little is known about the chemical properties of At and microsolvated At^- in particular [28, 31]. This neglection of the heaviest halide extends even to theoretical and computational studies, except for a force held molecular dynamics work comparing the entire series from F^- to At^- [16].

Microsolvation may be taken as "the stabilization of solute↔solvent complexes because of the explicit intermolecular interactions between the participating moieties" [38, 39]. Thus, two fundamental issues must be addressed: a rigorous sampling of the corresponding structural possibilities and an in-depth analysis of the involved intermolecular interactions. In addition, for the particular case of the heavy halides, relativistic effects must be properly treated [40, 41]. In this work, we attend to the points just exposed and study the structural, energetic, and bonding aspects involved in the microsolvation of heavy halides (Br^-, I^-, At^-) with up to six water molecules. To this end, we use a sound stochastic approach to exhaustively sample the energy landscapes and locate equilibrium geometries. We derive bonding information by analyzing the electron densities and use four component relativistic calculations to accurately assess relativistic effects.

2 | METHODS

We studied microsolvation of heavy halides by explicitly considering individual water molecules in $[X(H_2O)_n]^-$ clusters with X = Br, I, and At, and n = 1–6. Each PES was explored using the ASCEC algorithm [42–44], which produces candidate structures for local and global minima by following the evolution under annealing conditions of a system containing all molecules under consideration (water, X^-) initially placed at the center of a cubic box (to avoid structural bias) of predetermined length. The structures afforded by ASCEC were then optimized and characterized as true minima using Hartree–Fock and full (not frozen core) Moller–Plesset second order perturbation theory (MP2) in conjunction with the def2-TZVPPD basis set for all atoms [45, 46], and def2-TZVPPD pseudopotentials for I [47], and At [47], as implemented in the Gaussian09 suite of programs [48]. We refer to this particular model chemistry as HF and MP2 with pseudopotentials, or, more succinctly, as PP–HF and PP–MP2, respectively. The geometries thus obtained, which afforded the same geometrical motifs for the global minima in both PP frames, were used to study both, electron correlation and relativistic effects. All geometry optimization and relativistic calculations were carried out using the DIRAC17 code [49]. No symmetry constraints were imposed when optimizing molecular geometries at any level.

Accurate treatment of relativity is quite challenging. For this, we took the 18 PP global minima and reoptimized them using the four component Dirac–Hartree–Fock (DHF) Hamiltonian in conjunction with the Sadlej-pVTZ basis set in all cases (O, H [50], Br [51], I [52]) except for those containing At, for which the dyall.acv2z basis set was used in all atoms [53]. Nuclei were treated as Gaussian distributions. We refer to those calculations as relativistic DHF, or simply as 4c-DHF. The geometries thus obtained were then used to calculate binding energies at the full (all electron and full virtual space) 4c relativistic MP2 level, which we refer to as 4c-MP2. In order to assess the reliability of the dyall.acv2z basis set in the calculation of binding energies within 4c relativistic MP2, Table S3 shows negligible changes for all global minima containing up to three water molecules with respect to the dyall.acv3z results. Accordingly, in Table 4 we list binding energies for all systems using dyall.acv2z.

For each molecularity n, at the PP level, sequential binding energies BE^{XWn}, sequential hydration enthalpies ΔH^{XWn}, and sequential hydration Gibbs free energies ΔG^{XWn}, were calculated as statistical averages using as weighting factors the Boltzmann derived populations at 298 K and 1 atm (we refer to these as room conditions in what follows) for every single minimum within the given PES. For each isomer i within each molecularity n, the corresponding quantities sequential BE_i^{XWn}, sequential ΔH_i^{XWn}, sequential ΔG_i^{XWn} were calculated considering the energetics of the $[X(H_2O)_{n-1}]^- + H_2O \rightarrow [X(H_2O)_n]^-$ reaction with X = Br, I, and At. In all cases, electronic energies were corrected for zero-point vibrational energies (ZPEs).

Bonding interactions were dissected using the tools provided by the quantum theory of atoms in molecules (QTAIM) [54] calculated using the AIMStudio13 program [55]. Thus, for bond critical points (BCPs) corresponding to intermolecular interactions on the PP PES, we gathered information from the electron density $\rho(\mathbf{r}_c)$, its Laplacian $\nabla\rho(\mathbf{r}_c)$, and the potential $V(\mathbf{r}_c)$, kinetic $G(\mathbf{r}_c)$, and total $H(\mathbf{r}_c) = V(\mathbf{r}_c) + G(\mathbf{r}_c)$ energy densities. For comparative purposes, this analysis was made using the PP geometries and densities derived from the HF, MP2 model chemistries described above.

3 | RESULTS AND DISCUSSION

3.1 | Structures and energies

As seen in Table 1, at the PP–MP2 level, there is a rich structural diversity for the microsolvation of heavy halides, with multitudes of local minima spanning small energy windows. All the equilibrium structures for the three halides with 1, 2, and 3 water molecules are shown in Figure 1. Due

to the large structural complexity for the microsolvation of the halides with 4, 5, and 6 water molecules, just a few hand-picked geometrical motifs common to the three halides are shown in Figure 1. The entire set of 272 equilibrium geometries located in this work is available in the Supporting Information. Boltzmann distributions indicate that for each molecularity, multiple isomers, as opposed to just the lone global minimum, do contribute to experimental observables. To deal with this large number of isomers, we devised the following notation: structures are addressed as W_nS_m, where W_n stands for the number of water molecules and S_m indicates the relative stability within each PES; thus, for example, W_3S_2 describes the second lowest energy (just above the global minimum) structure for the cluster containing three water molecules.

Our stochastic search recovers all known geometrical motifs. In addition, several molecular arrangements for the microsolvation of heavy halides are reported here for the first time in the scientific literature. Fittingly, ZPE-corrected electronic binding energies listed in Table 2 indicate that halide↔water complexes are energetically stable with respect to the isolated components. As might be rationalized from an electrostatic perspective, Br^- has a less shielded charge than I^-, At^-, accordingly, more negative binding energies, suggesting stronger interactions in Br containing clusters within each molecularity, are found. Conversely, there does not seem to be much of a difference in the shieldings between the charges in I^-, At^-. In the same line of reasoning, it is clear that heavy halides exhibit smaller magnitudes in microsolvation energies when compared to other singly charged anions such as F^-, for which BE ∈ [−24, −100] kcal/mol (with 1–6 molecules of water), [39] and cations such as Li^+, BE ∈ [−62, −115] kcal/mol (with 3–5 molecules of water), [56] and $[CH_3Hg]^+$, BE ∈ [−32, −65] kcal/mol (with 1–3 molecules of water) [57].

Shuffling of the relative energetic ordering upon inclusion of entropy, temperature, and internal degrees of freedom is not only a common occurrence but should be expected when analyzing molecular clusters. The reason is well understood: as temperature raises, individual molecules within a given cluster increase their kinetic energies and thus the number of intermolecular contacts decreases until eventually, at high enough temperatures (case dependent), ideal gas behavior (no intermolecular interactions at all) is attained. Consequently, in general, less compact, more open structures are favored in the Gibbs free energy ordering, as clearly shown in section 2.2 of the Supporting Information, where severe changes with respect to the purely electronic energies are seen, such that in one case the identity of the global minimum is changed. Additional support for this view is obtained if quantum topology instead of Euclidean geometry is used to determine dimensionality of molecular structures [58], thus, regardless of the spatial distribution of the atoms, a cluster is considered one dimensional under the quantum topology criterion, $1D_{QT}$, if only bond critical points are found after analysis of the topology of the electron density, $2D_{QT}$ clusters contain at least one ring critical point, and $3D_{QT}$ clusters contain at least one cage critical point. As illustrative examples, structure W_5S_{26}, having no cage critical points, is a $2D_{QT}$ rather than a $3D_{QT}$ cluster and climbs from the 26th position in the electronic energy hierarchy to the second spot in the free energy scale.

TABLE 1 Summary of the structural and energetical features derived from the PP–MP2 potential energy surfaces for the microsolvation of heavy halides $[X(H_2O)_n]^-$ with X = Br, I, and At, and n = 1–6

	Structural motifs			Relative energy ranges (kcal/mol)		
n	$[Br(H_2O)_n]^-$	$[I(H_2O)_n]^-$	$[At(H_2O)_n]^-$	$[Br(H_2O)_n]^-$	$[I(H_2O)_n]^-$	$[At(H_2O)_n]^-$
1	1	1	1	–	–	–
2	1	1	1	–	–	–
3	6	6	6	4.93	4.50	4.42
4	12	16	15	6.06	6.21	6.31
5	31	26	25	7.83	6.69	7.42
6	53	34	36	8.99	8.79	9.79

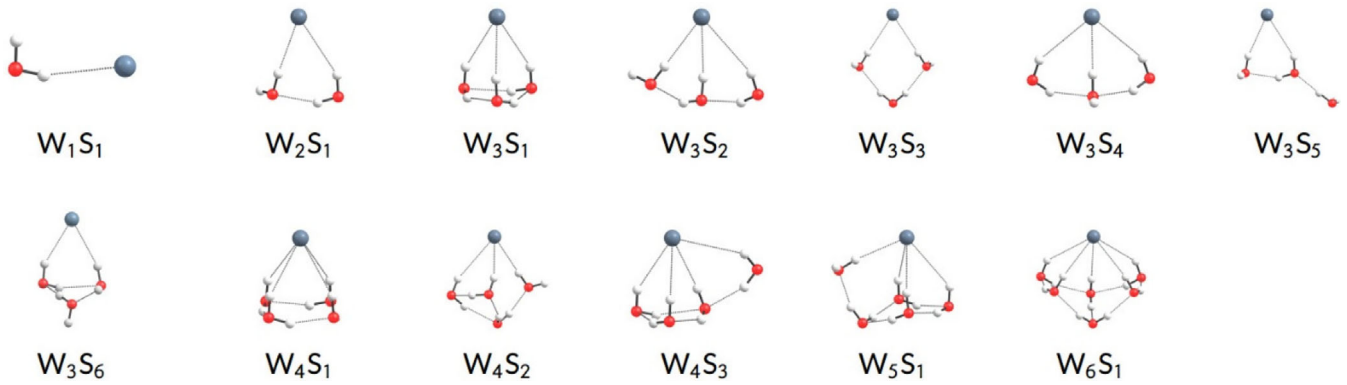

FIGURE 1 Structural diversity for $[X(H_2O)_n]^-$ clusters; X = Br, I, At, n = 1–6. All the structures for n = 1–3, and just a few lowest energy geometrical motifs common to the three halides for n = 4–6 are shown (see Supporting Information for a complete list of isomers and populations). For the complete set of structures, relative stabilities among the isomers change as a function of the identity of the halide as seen in the entire set of structures included in the Supporting Information

	BE		
n	$[Br(H_2O)_n]^-$	$[I(H_2O)_n]^-$	$[At(H_2O)_n]^-$
1	−12.82	−10.80	−10.29
2	−12.22	−10.86	−10.56
3	−12.71	−11.92	−11.78
4	−11.68	−11.51	−11.54
5	−10.43	−9.78	−9.61
6	−11.16	−10.87	−10.94

TABLE 2 Sequential PP–MP2 binding energies (kcal/mol) for the microsolvation of heavy halides using statistical weighted averages accounting for the contributions from all clusters considering the $[X(H_2O)_{n-1}]^- + H2O \rightarrow [X(H_2O)_n]^-$ reaction; X = Br, I, and At

TABLE 3 Sequential PP–MP2 hydration enthalpies (ΔH, kcal/mol) and hydration Gibbs energies (ΔG, kcal/mol) at room conditions for the microsolvation of heavy halides

	ΔH (kcal/mol)					ΔG (kcal/mol)				
	$[Br(H_2O)_n]^-$		$[I(H_2O)_n]^-$		$[At(H_2O)_n]^-$	$[Br(H_2O)_n]^-$		$[I(H_2O)_n]^-$		$[At(H_2O)_n]^-$
n	This work	Previous	This work	Previous	This work	This work	Previous	This work	Previous	This work
1	−12.13	−11.7[a], −12.6[b]	−10.01	−10.3[a], −10.2[b]	−9.46	−7.54	−7.3[a], −5.97[c]	−5.73	−5.4[b]	−5.29
2	−12.92	−11.6[a], −12.3[b]	−11.54	−9.5[a], −10.2[b]	−11.23	−4.01	−6.3[a], −3.93[c]	−2.65	−4.2[b]	−2.37
3	−13.79	−11.4[a], −11.5[b]	−13.04	−9.2[a], −9.4[b]	−12.88	−2.81	−4.6[a], −1.25[c]	−2.01	−3.1[b]	−1.81
4	−12.41	−11.0[a], −10.9[b]	−12.28	−9.2[a]	−12.34	−2.46	−3.2[a], −4.24[c]	−1.99	–	−2.07
5	−11.23	−10.8[a]	−10.42	−9.0 [a]	−10.26	−1.11	–	−0.58	–	−0.78
6	−12.06	−10.3[a]	−11.81	–	−11.83	−1.65	–	−1.46	–	−0.96

Note: All energies were calculated using statistical weighted averages accounting for the contributions from all clusters for a given molecularity.
[a]Experimental [2].
[b]Experimental [1].
[c]Calculated [15].

Experimental sequential hydration enthalpies and hydration Gibbs energies at room conditions are available for the microsolvation of heavy halides at the molecularities studied in this work [1, 2]. We list them along with our computed results in Table 3 and plot them as a function of the number of water molecules in Figure 2, from which we draw the following observations: (i) As the number of water molecules increases, sequential Gibbs hydration energies decrease in magnitude regardless of the identity of the halide, suggesting an asymptotic stabilization on the magnitude of the hydration free energy as *n* grows larger, as is expected when the bulk limit is approached. (ii) When available, experimental measurements of sequential formation enthalpies are quite consistent with each other and our results match them quite well (see Table 3).

We focus now on the important point of the preferred location of the anion. Roughly speaking, among the 272 equilibrium structures reported in this work (see Figure 1, as well as the Supporting Information), there are two general categories of structural possibilities depicted in Figure 3: superficial, in which the halide sits in the periphery of a water cluster, interacting with the external protons, or internal, in which water molecules surround the halide. At the low molecularities treated in this work, the vast majority of structures correspond to superficial arrangements, with the only exceptions of W_5S_{26}, W_6S_{22}, and W_6S_{24} in the microsolvation of bromide, which exhibit internal arrangements. This superficial structural preference arises because the collective interactions leading to the formation of small water clusters outweighs the strength of direct halide↔water contacts.

The observed preference for superficial arrangements in the microsolvation of Br^-, I^-, At^- is consistent with the Cl^- case [7, 9], but is in stark contrast with the preferred internal structures in the microsolvation of F^-, the smallest halide [39]. This structural preference may be taken as indicative of a reduction of the effective charge as the atomic number of the halide increases, to the point that water to water hydrogen bonding becomes the dominant (over halide to water) interaction for the heavier X.

The size of the basis set plays an important role in the calculation of binding energies in molecular clusters, leading to the well-known basis set superposition error (BSSE). For the specific case of the microsolvation of halides, Kim and coworkers [59] have suggested using only 50% of the obtained BSSE corrections to accurately estimate interaction energies. Using this procedure, we corrected the binding energies for the $[X(H_2O)_n]^-$ clusters up to $n = 3$ using the counterpoise method [60] and found that uncorrected binding energies are overestimated with respect to corrected energies by no more than ∼8% and that there is no shuffling of relative energies. See the Supporting Information for a detailed

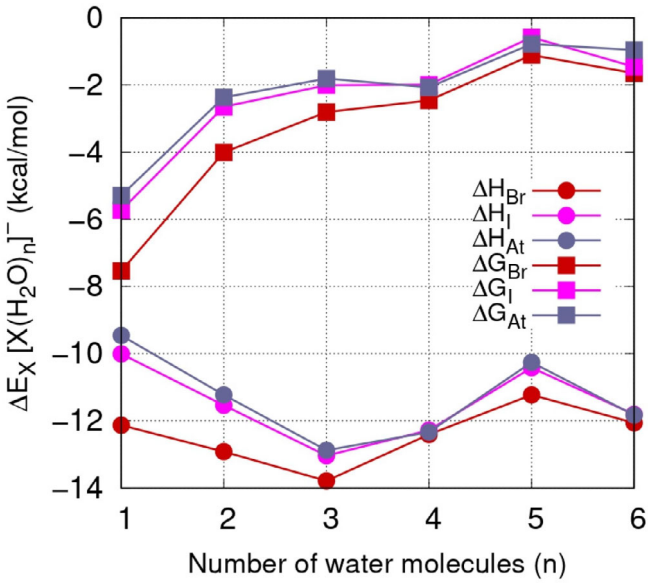

FIGURE 2 Sequential PP–MP2 formation enthalpies and Gibbs energies as a function of *n*, the number of water molecules microsolvating the heavy halides

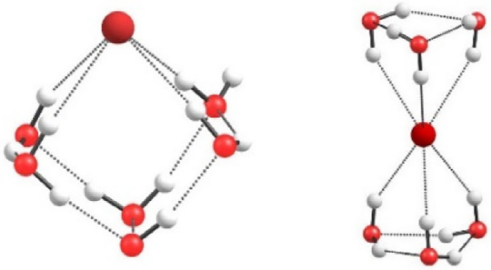

FIGURE 3 Examples of superficial (left) and internal (right) positioning of the halide in the title clusters

description of the calculations and results. Notice that the use of full MP2 has been shown to lead to wrong BSSE corrected binding energies in closely related systems [61]. To address this issue, we used the MP2(full) optimized geometries and corrected for the BSSE under both full and frozen core approaches for all clusters in the *n* = 1–3 stoichiometries and obtained discrepancies no larger than 4% in binding energies.

3.2 | Dissection of bounding interactions

Intermolecular bonding interactions may be studied invoking several aspects, in particular, we focus here on the identity of the interacting atoms, in the interaction distances, and in the topological properties of the electron densities. Because of the identity of the interacting atoms, two different types of intermolecular contacts emerge: water (proton) to halogen, HOH···X, and water to water HOH···OH_2 hydrogen bonding. In the HOH···X cases, individual water molecules in direct contact with the X atom may be subdivided according to their roles in HBs with other waters (their ability to accept or to donate electron density, from or to other water molecules) as (a) double donors, (b) donors, (c) no water↔water HBs, (d) donor and acceptors, and (e) acceptors of electron density, as illustrated at the top of Figure 4. Noticeably, the chemical environment affects the nature of the H···X interaction to the extent that each family of water molecules, (a)–(e), comprises a well-defined range of distances and a well-defined area under the curve, thus, going from left to right on individual plots in Figure 4 equates to increasing the electron density at the particular water molecule in direct contact with X.

Vertical lines in Figure 4 mark the bond distances corresponding to the intersections with the $|V(\mathbf{r}_c)|/G(\mathbf{r}_c) = 1$ boundary that according to Espinosa and coworkers [62] separates closed shell (ionic or non-covalent long distance to the right of the vertical line, both present in our case) interactions from the intermediate (contributions from both long range and covalent to the left of the vertical lines) character contacts. This boundary is rooted in solid grounds because at bond critical points $|V(\mathbf{r}_c)|/G(\mathbf{r}_c) < 1$ indicates a local dominance of the repulsive electronic kinetic energy term, thus displacing electron density away from the BCP toward the nuclei, and, conversely, $|V(\mathbf{r}_c)|/G(\mathbf{r}_c) > 1$ indicates a local dominance of the attractive electronic potential energy term, thus accumulating electron density in the vicinities of the BCP. Evidently, for all X and molecularities, closed shell and intermediate character H···X interactions are found. H···X interactions of intermediate character have contributions from covalency ($|V(\mathbf{r}_c)|/G(\mathbf{r}_c) > 1$, shorter distances) only for those cases in which the water molecules donate electron density to other water molecules via formation of hydrogen bonds.

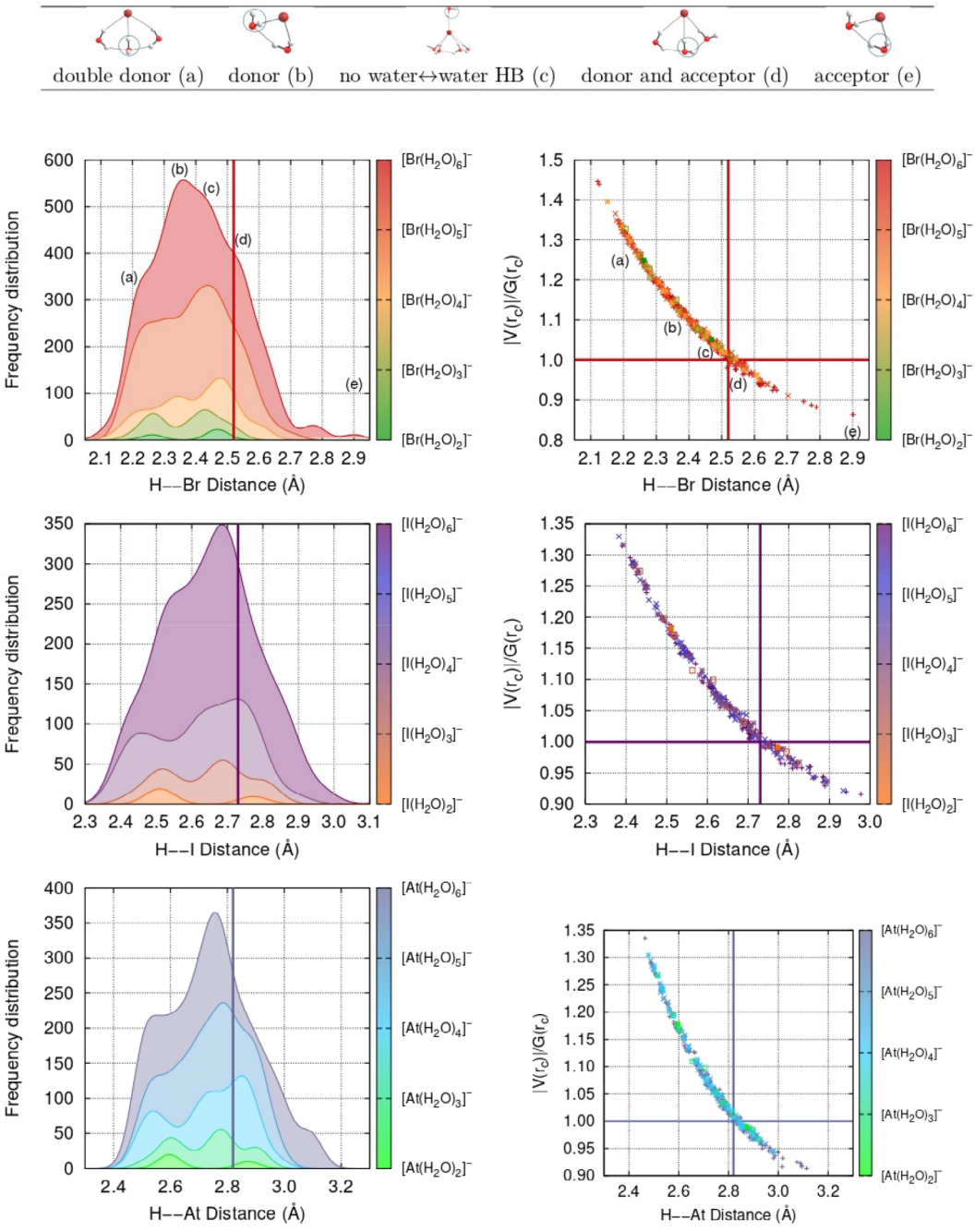

FIGURE 4 Radial distributions (left) and ratio of the potential to kinetic energy densities at bond critical points [62] (right) as a function of the intermolecular H···X distances in the $[X(H_2O)_n]^-$ clusters. Vertical lines separate long range interactions (to the right of the line) from intermediate character interactions (to the left of the line) as a function of the H···X distance according to the intersection with the $|V(\mathbf{r}_c)|/G(\mathbf{r}_c) = 1$ boundary. All molecularities and all halides are included. Data taken from the PP–MP2 optimized geometries. The structures at the top illustrate water molecules according to their abilities to accept or to donate electron density to other water molecules

3.2.1 | Effects of the formal change and identity of the halide

Using the data collected in Figure 5 we analyze the effects of both, the formal charge and the identity of the halide in the surrounding water to water, and halide to water hydrogen bonding networks. As a general rule, X^- has a chaotropic effect, [64] increasing HOH···OH_2 distances (left top panel in Figure 5), thus, if the premise that interaction strength correlates inversely with H···O distances is accepted, then, as a whole, it is inferred that heavy halides debilitate the surrounding HB network. HOH···X interactions are dependent on the identity of the halide as is seen in the bottom left panels of Figure 5.

The concentration of electron density in the vicinities of the bond critical points exhibits an exponential decay for both HOH···OH_2 and H···X interactions (top and bottom right panels in Figure 5). This exponential decay, which correctly describes the asymptotic limit of vanishing electron densities for infinite distances, has previously been noticed in closely related hydrogen bond networks [62, 65–67]. It is interesting to notice that while the three halides affect in the same qualitative way the electron densities of the bond critical points for water to water hydrogen bonds (top right panel in Figure 5), electron densities, and by extension the nature and strength of the interactions in H···X contacts are quite more sensitive to the identity of the halide (bottom right panel in Figure 5). To illustrate this point, consider, for example, a vertical line say at ≈2.8 Å in the bottom right panel of Figure 5: it is seen that for the same interaction distance, H···Br BCPs accumulate less electron density than H···I and that H···At BCPs, thus, H···Br contacts may be thought as being weaker and as having a smaller covalent character; however, this is just a consequence of the heavier atoms having more electrons away from the nucleus, the real evidence that Br···H interactions are stronger is provided by the shorter bond distances with larger accumulations of electron densities at the top left corner of the plot.

As discussed above, all OH···OH_2, H···X interactions are classified using the criteria suggested by Espinosa and coworkers [62] as purely closed shell (ionic or long range) or as of intermediate character with contributions from both closed shell and covalent interactions. Further insight into the nature of the interactions might be obtained by analyzing the signs of both the Laplacian of the electron density and the total energy densities at bond critical points. Formally $\nabla^2\rho(\mathbf{r}_c) > 0$ characterize local minima in electron density while $\nabla^2\rho(\mathbf{r}_c) < 0$ indicate local maxima. Thus, negative Laplacians describe local concentration of electron density around the associated BCP, which is a strong indicator of covalent interactions. Conversely, positive Laplacians describe local depletion of charge around the associated BCP, which is consistent with closed shell (again, ionic or long range) interactions. In addition, the local total energy density is the sum of the local potential and kinetic energy densities as given by $H(\mathbf{r}_c) = G(\mathbf{r}_c) + V(\mathbf{r}_c)$. Therefore, negative total local energy densities at BCPs indicate a local dominance of the always negative and attractive potential energy and thus characterizes locally stabilizing interactions that favor the accumulation of electron density. Conversely, positive total local energy densities at BCPs characterize locally destabilizing interactions because of the local dominance of the always positive and repulsive kinetic energy which disfavors the local accumulation of electron density. Figure 6 shows plots of the variations of the Laplacians of the electron densities and the $|V(\mathbf{r}_c)|/G(\mathbf{r}_c)$ ratio as a function of the so called bond parameter, $H(\mathbf{r}_c)/\rho(\mathbf{r}_c)$ for all OH···OH_2, H···X interactions. There is a nice mapping between the local ratio of potential to kinetic energy and the local total energy density (right panels, Figure 6), that is, positive values of H relate closed shell interactions while negative values of H relate to intermediate character interactions. The signs of the Laplacians of the electron densities at BCPs (right panels, Figure 6) are more problematic as they are always positive thus describing only local depletion of charge,

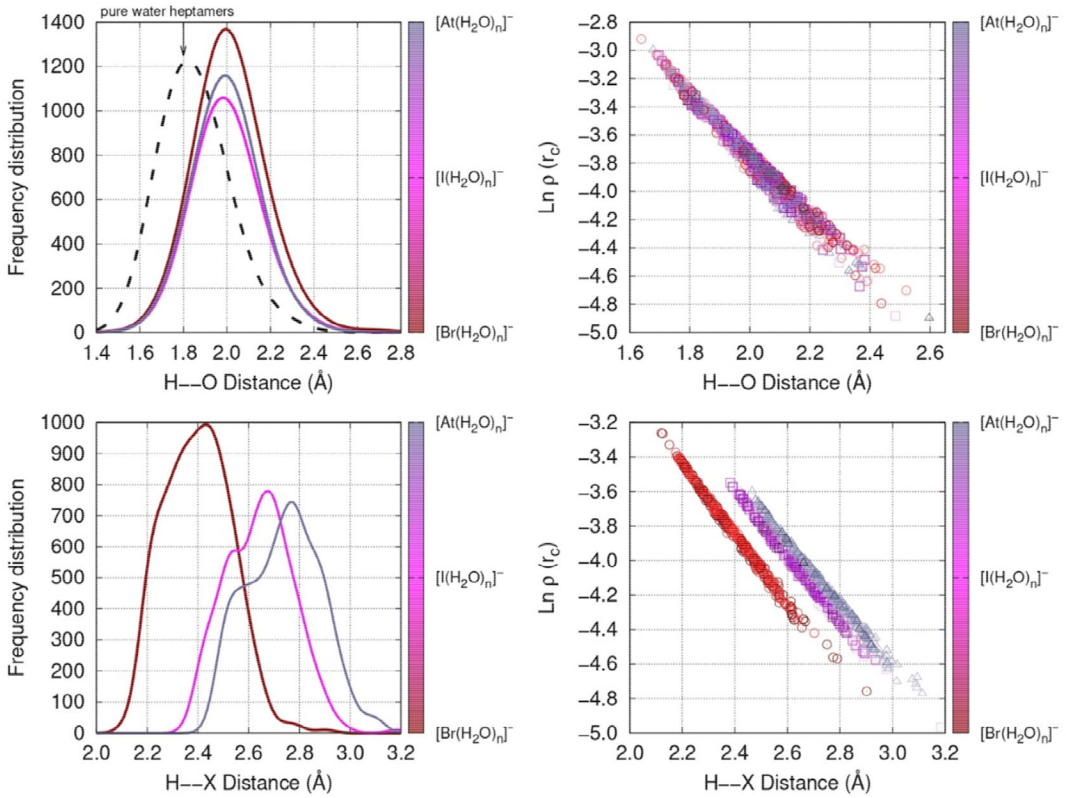

FIGURE 5 Radial distributions (left) and exponential decays for the electron densities at bond critical points for the HOH···OH_2. (top) and HOH···X (bottom) interactions. The radial distribution for the pure water heptamers [63] is included for comparison

however, a sizable number of bond critical points have negative total energy densities, suggesting that despite the local minima in electron density character, the interaction is still stabilizing. This apparent inconsistency between the signs of the Laplacians and the signs of the total energy densities at bond critical points is well documented [57, 66, 68].

3.2.2 | Ionicity and covalency

Thus far, our analysis of bonding interactions follows popular QTAIM based criteria that impose stern and clear boundaries between closed shell, intermediate, and covalent character such as the $|V(\mathbf{r}_c)|/G(\mathbf{r}_c)$ ratio [62] and the signs of the Laplacians of the electron densities and of the total energy densities, all evaluated at the corresponding bond critical points. However, as we pointed out above, inconsistencies are found among the several criteria. These inconsistencies, arise because in this view (which appears to have permeated the general public), ionic and covalent interactions are taken as two separate excluding features of chemical bonding. Our results lead us to argue, just like Pauling [69] and Coulson [70] did in the early days of theoretical descriptions of chemical bonds, that instead of being opposite antagonistic factors, ionicity and covalency ought to be considered as contributing parts, whose weights are to be determined for each particular interaction. Here, we assign ionic and covalent character to simple meaningful descriptors as suggested elsewhere [39]. Thus, for a given interaction involving A···B atoms, we calculate an ionicity factor (IF) by quantifying the Coulomb interaction between the atoms as $IF_{A\cdots B} = |q_A q_B|/r_{A\cdots B}$. In the same line, covalency is quantified by measuring the amount of electron density surrounding the cofresponding bond critical point. We provide in Figure 7 a 3-dimensional plot relating the variation of the $|V(\mathbf{r}_c)|/G(\mathbf{r}_c)$ ratio [62] as a function of both, ionicity and covalency, for the large number of H···X, HOH···OH_2 interactions (>400 for each halide) found in this work. Our preceding argument in favor of covalency and ionicity both contributing to intermolecular interactions is backed up by the evidence in this plot: it is clear that increasing the $|V(\mathbf{r}_c)|/G(\mathbf{r}_c)$ ratio is the result of simultaneously increasing both covalency and ionicity and not, as might naively be expected, by an increasing contribution from covalency concomitant with a decreasing contribution of ionicity.

3.3 | Relativistic treatment

As stated in the Section 2, the 18 global minima obtained with the PP–HF and PP–MP2 methods were reoptimized at the 4c-DHF level to assess relativistic effects. Cartesian coordinates for the resulting structures are provided in the Supporting Information. As a general rule, changing the level of theory leads to changes in interaction distances but not in connectivity among the interacting moieties.

The effect of electron correlation in the nature of bonding interactions may be assessed from Figure 8. Overall, electron correlation seems to increase the $|V(\mathbf{r}_c)|/G(\mathbf{r}_c)$ ratios for a given interaction distance; thus, as discussed above, leading to a concomitant increase in both, ionic and covalent contributions to the corresponding contact. In fact, PP–HF calculations seem to place all interactions (with a few exceptions) in the closed range category, while PP–MP2 affords a sizable number of intermediate character interactions.

As seen in Figure 9, HOH···H_2O distances are less sensitive to relativistic effects than H···X. Remarkably, ignoring electron correlation seems to be a larger source of error than ignoring relativistic effects in the calculated bond lengths for intermolecular interactions. From an energetic

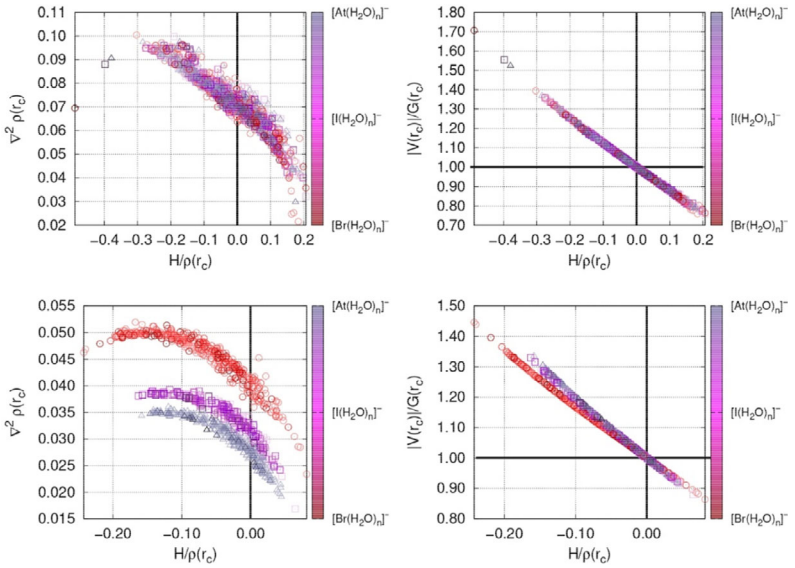

FIGURE 6 Laplacian of the electron density at bond critical points (left) the $|V(\mathbf{r}_c)|/G(\mathbf{r}_c)$ ratio [62] (right) as a function of the bond parameter for HOH···OH_2 (top) and H···X (bottom) interactions in the microsolvation of heavy halides. Data taken from the PP–MP2 optimized geometries

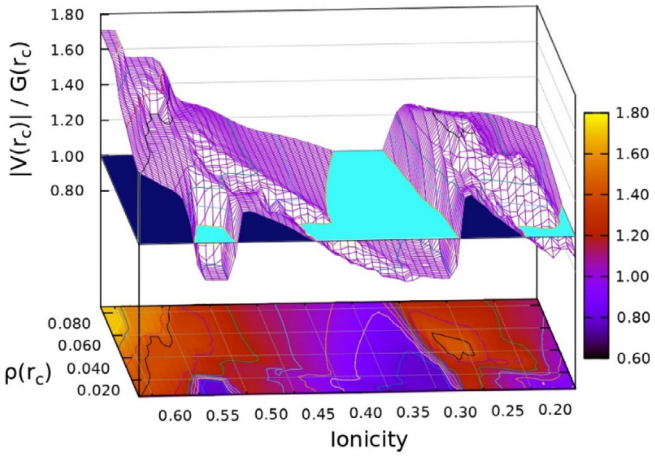

FIGURE 7 Variation of the $|V(\mathbf{r}_c)|/G(\mathbf{r}_c)$ ratio [62] as a function of both, the ionic and covalent character for intermolecular interactions in the microsolvation of heavy halides. Two regimes are seen, those for ionicities below 0.30 correspond to X···H interactions while larger ionicities correspond to H_2O···HOH contacts. The plane at $|V(\mathbf{r}_c)|/G(\mathbf{r}_c) = 1$ marks the boundary between closed shell (long range, ionic) and intermediate (contributions from closed shell and from covalent) interactions

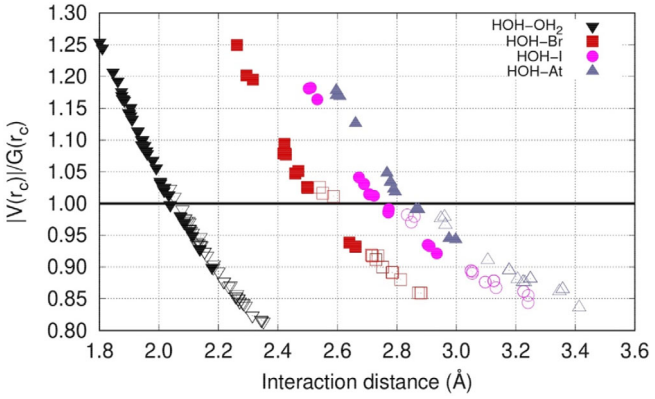

FIGURE 8 Variation of the $|V(\mathbf{r}_c)|/G(\mathbf{r}_c)$ ratio [62] as a function of the interaction distance for all intermolecular interactions in the microsolvation of heavy halides. Filled symbols correspond to PP–MP2 calculations, open symbols correspond to PP–HF calculations

perspective, neglecting relativistic and electron correlation effects leads to underestimation of the strengths of the interactions, with the exception of BEs of At^- containing clusters, for which HF values are very close to the DHF ones. In more detail, relativistic effects on BEs are not negligible, they depend on whether electron correlation is included or not. As shown in Table 4, for $n = 1$ in the Iodine case, correlation effects within a relativistic regime are around −2.30 kcal/mol or larger than −20%, notice that these values are calculated on the same DHF optimized geometry. On the other hand relativistic effects under MP2 are close to +1.30 kcal/mol or larger than 12%, notice that it is not possible to obtain relativistic MP2 geometries. Correlation and relativistic effects are of different sign.

4 | SUMMARY AND CONCLUSIONS

The main findings in this work may be summarized as follows:

1. The PES reported here for the microsolvation of heavy halides exhibit a rich structural variety, with several individual clusters contributing to experimental measurements. A good number of structures are reported here for the first time in the scientific literature.
2. There is a marked preference for superficial arrangements where the X atom sits in the periphery of the cluster interacting with protons external to the water hydrogen bonding network, thus revealing the importance of water to water hydrogen bonding in the microsolvation of heavy halides.
3. Intermolecular interactions in the microsolvation of heavy halides are characterized in this work as closed shell (ionic, long range) on one hand, and as of intermediate character with contributions from both, closed shell and covalent interactions, on the other.
4. The nature of the X···HOH interactions is determined by the role played by individual water molecules (in direct contact with the X atom) in water to water hydrogen bonding. Five distinct types of water molecules are identified: double donors of electron density, donors of electron density, donor and acceptor of electron density, no water to water hydrogen bonding, and acceptor of electron density.
5. The strength of X···HOH interactions decreases with the size (nuclear mass) of the halide. Conversely, the strength of the surrounding H_2O···HOH network grows with the size of the halide.

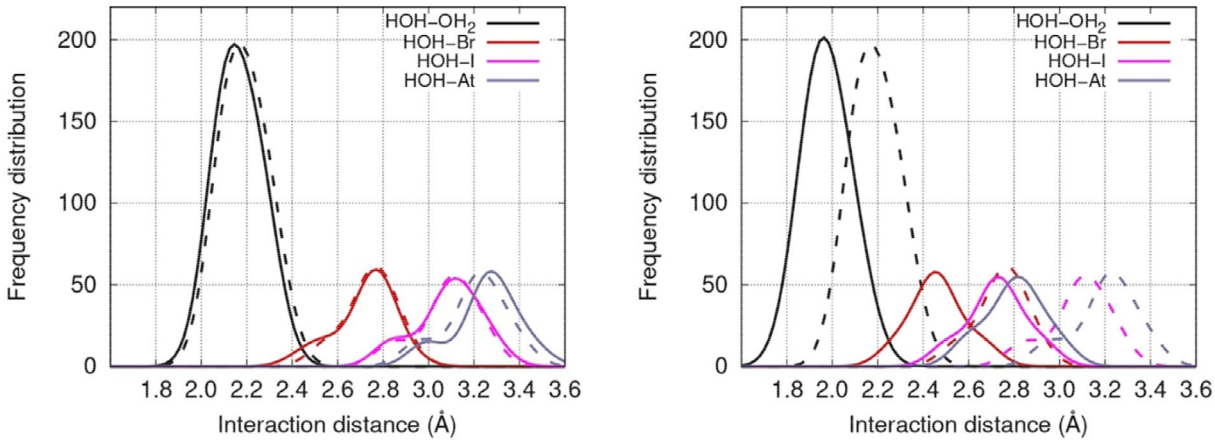

FIGURE 9 Radial distributions of the H···X, HOH···OH_2 interaction distances in the microsolvation of heavy halides with up to six water molecules. Solid lines in the left panel correspond to the 4c-DHF relativistic calculations. Solid lines in the right panel correspond to PP–MP2 calculations. In both panels, dashed lines correspond to PP–HF

TABLE 4 Binding energies (difference in energy between the clusters and the isolated components in kcal/mol) for the microsolvation of heavy halides under different model chemistries

	$[Br(H_2O)_n]^-$				$[I(H_2O)_n]^-$				$[At(H_2O)_n]^-$			
n	PP–HF…	PP–MP2	…4c-DHF	…4c-MP2	PP–HF	PP–MP2	4c-DHF	4c-MP2	PP–HF	PP–MP2	4c-DHF	4c-MP2
1	−9.99	−13.95	−10.06	−12.54	−8.19	−11.81	−8.19	−10.50	−7.63	−11.25	−7.43	−9.72
2	−20.13	−28.51	−20.39	−25.80	17.00	−24.98	17.18	−22.42	−16.04	−24.09	−15.78	−21.28
3	−30.81	−44.52	−31.45	−40.50	−26.74	−40.15	−27.27	−36.37	−25.47	−39.07	−25.27	−35.13
4	−40.52	−58.93	−41.48	−53.89	−35.97	−54.32	−36.79	−49.28	−34.55	−53.24	−34.53	−48.14
5	−49.27	−72.07	−50.06	−65.07	−43.85	−66.63	−44.94	−60.33	−42.23	−65.48	−42.20	−59.02
6	−58.18	−86.19	−59.78	−78.55	−52.29	−80.58	−53.73	−72.95	−50.45	−79.28	−50.54	−71.60

Note: Only the global minimum for each molecularity is considered. Molecular geometries were fully optimized at the level indicated by each column heading, except for the 4c-MP2 values, which were computed over the 4c-DHF geometries (see the Section 2).

6. Increasing the $|V(\mathbf{r}_c)|/G(\mathbf{r}_c)$ ratio in the [1, 2] interval is a consequence of a simultaneous increase in ionicity and covalency in the corresponding intermolecular interaction.
7. For the microsolvation of heavy halides, electron correlation and relativistic effects are of opposite signs and of the same order of magnitude, though electron correlation effects are larger.
8. In general, improper treatment of electron correlation and relativity leads to underestimation of binding energies and overestimation of interaction distances.
9. We report here for the first time in the scientific literature the microsolvation of At^- under exhaustive samplings of the configurational spaces using rigorous ab initio and relativistic methods. It appears that the properties of $[At(H_2O)_n]^-$ do not deviate from the trends expected for the series of halides.
10. We found that the Def2 pseudopotential is not working well in the reproduction of binding energies of a few motifs of microsolvated halides.

ACKNOWLEDGMENTS

The work in Colombia was partially supported by Colciencias, Project 111571249844, and by University of Antioquia via "Estrategia para la sostenibilidad." Yuly Chamorro thanks University of Antioquia for her graduate scholarship. The work in Argentina was supported by Argentinian Research Council on Science and Technology, CONICET (Grant PIP112-201301-00361), and by the Argentinian Agency for Promotion of Science and Technology, FONCYT (Grant PICT2016-2936).

AUTHOR CONTRIBUTIONS

Yuly Chamorro: Conceptualization; formal analysis; investigation; methodology; validation; visualization; writing-original draft; writing-review and editing. **Edison Florez:** Conceptualization; formal analysis; investigation; methodology; validation; visualization; writing-original draft; writing-review and editing. **Alejandro Maldonado:** Formal analysis; investigation; validation; visualization; writing-original draft; writing-review and editing. **Gustavo Aucar:** Conceptualization; formal analysis; funding acquisition; methodology; resources; software; validation; writing-review and editing. **Albeiro Restrepo:** Conceptualization; formal analysis; funding acquisition; methodology; project administration; resources; software; supervision; writing-original draft; writing-review and editing.

ORCID

Gustavo Aucar https://orcid.org/0000-0003-2547-2330
Albeiro Restrepo https://orcid.org/0000-0002-7866-7791

REFERENCES

[1] M. Arshadi, R. Yamdagni, P. Kebarle, *J. Phys. Chem.* **1970**, *74*, 1475.
[2] K. Hiraoka, S. Mizuse, S. Yamabe, *J. Phys. Chem.* **1988**, *92*, 3943.
[3] G. Markovich, R. Giniger, M. Levin, O. Cheshnovsky, *J. Chem. Phys.* **1991**, *95*, 9416.
[4] P. Ayotte, G. H. Weddle, J. Kim, M. A. Johnson, *J. Am. Chem. Soc.* **1998**, *120*, 12361.
[5] L. Piatkowski, Z. Zhang, E. H. Backus, H. J. Bakker, M. Bonn, *Nat. Commun.* **2014**, *5*, 4083.
[6] M. Antalek, E. Pace, B. Hedman, K. O. Hodgson, G. Chillemi, M. Benfatto, R. Sarangi, P. Frank, *J. Chem. Phys.* **2016**, *145*, 044318.
[7] J. E. Combariza, N. R. Kestner, J. Jortner, *J. Chem. Phys.* **1994**, *100*, 2851.
[8] R. Ayala, J. M. Martínez, R. R. Pappalardo, M. E. Sánchez, *J. Phys. Chem. A* **2000**, *104*, 2799.
[9] H. M. Lee, D. Kim, K. S. Kim, *J. Chem. Phys.* **2002**, *116*, 5509.
[10] R. Ayala, J. M. Martínez, R. R. Pappalardo, M. E. Sánchez, *J. Chem. Phys.* **2003**, *119*, 9538.
[11] M. Masamura, *J. Chem. Phys.* **2003**, *118*, 6336.
[12] A. Likholyot, J. K. Hovey, T. M. Seward, *Geochim. Cosmochim. Acta* **2005**, *69*, 2949.
[13] S. G. Neogi, P. Chaudhury, *J. Comput. Chem.* **2013**, *34*, 471.
[14] D. Arismendi-Arrieta, M. Riera, P. Bajaj, R. Prosmiti, F. Paesani, *J. Phys. Chem. B* **2015**, *120*, 1822.
[15] H. Wen, T. Huang, Y. R. Liu, S. Jiang, X. Q. Peng, S. K. Miao, C. Y. Wang, Y. Hong, W. Huang, *Chem. Phys.* **2016**, *479*, 129.
[16] F. Réal, A. Severo Pereira Gomes, Y. O. Guerrero Martínez, T. Ayed, N. Galland, M. Masella, et al., *J. Chem. Phys.* **2016**, *144*, 124513.
[17] J. D. Mallory, V. A. Mandelshtam, *J. Phys. Chem. A* **2018**, *122*, 4167.
[18] P. Bajaj, M. Riera, J. K. Lin, Y. E. M. Montijo, J. Gazca, F. Paesani, *J. Phys. Chem. A* **2019**, *123*, 2843.
[19] D. R. Kester, I. W. Duedall, D. N. Connors, R. M. Pytkowicz, *Limnol. Oceanogr.* **1967**, *12*, 176.
[20] S. Hunt, M. Roeselova, W. Wang, L. Wingen, E. Knipping, D. Tobias, et al., *J. Phys. Chem. A* **2004**, *108*, 11559.
[21] D. Clifford, J. Donaldson, *J. Phys. Chem. A* **2007**, *111*(39), 9809.
[22] W. Simpson, R. Glasow, K. Riedel, P. Anderson, P. Ariya, J. Bottenheim, et al., *Atmos. Chem. Phys.* **2007**, *7*, 4375.
[23] L. J. Carpenter, S. M. MacDonald, M. D. Shaw, R. Kumar, R. W. Saunders, R. Parthipan, et al., *Nat. Geosci.* **2013**, *6*, 108.
[24] S. D. Richardson, A. D. Thruston, C. Rav-Acha, L. Groisman, I. Popilevsky, O. Juraev, V. Glezer, A. B. McKague, M. J. Plewa, E. D. Wagner, *Environ. Sci. Technol.* **2003**, *37*, 3782.
[25] M. J. Plewa, E. D. Wagner, S. D. Richardson, A. D. Thruston, Y. T. Woo, A. B. McKague, *Environ. Sci. Technol.* **2004**, *38*, 4713.
[26] E. Agus, N. Voutchkov, D. L. Sedlak, *Desalination* **2009**, *237*, 214.
[27] G. Vaidyanathan, M. R. Zalutsky, *Curr. Radiopharm.* **2008**, *1*, 177.
[28] A. Sabatié-Gogova, J. Champion, S. Huclier, N. Michel, F. Pottier, N. Galland, Z. Asfari, M. Chérel, G. Montavon, *Anal. Chim. Acta* **2012**, *721*, 182.
[29] J. Champion, A. Sabatié-Gogova, F. Bassal, T. Ayed, C. Alliot, N. Galland, G. Montavon, *J. Phys. Chem. A* **2013**, *117*, 1983.
[30] D. C. Sergentu, D. Teze, A. Sabatié-Gogova, C. Alliot, N. Guo, F. Bassal, I. D. Silva, D. Deniaud, R. Maurice, J. Champion, N. Galland, G. Montavon, *Chem. A Eur. J.* **2016**, *22*, 2964.
[31] N. Guo, F. Pottier, J. Aupiais, C. Alliot, G. Montavon, J. Champion, *Inorg. Chem.* **2018**, *57*, 4926.
[32] J. Styszyński, J. Kobus, *Chem. Phys. Lett.* **2003**, *369*, 441.
[33] J. Champion, M. Seydou, A. Sabatié-Gogova, E. Renault, G. Montavon, N. Galland, *Phys. Chem. Chem. Phys.* **2011**, *13*, 14984.
[34] T. Ayed, M. Seydou, F. Réal, G. Montavon, N. Galland, *J. Phys. Chem. B* **2013**, *117*, 5206.
[35] J. Pilmé, E. Renault, F. Bassal, M. Amaouch, G. Montavon, N. Galland, *J. Chem. Theory Comput.* **2014**, *10*, 4830.
[36] D. C. Sergentu, G. David, G. Montavon, R. Maurice, N. Galland, *J. Comput. Chem.* **2016**, *37*, 1345.
[37] D. Wilbur, *Curr. Radiopharm.* **2008**, *1*, 144.
[38] C. Hadad, E. Florez, N. Acelas, G. Merino, A. Restrepo, *Int. J. Quantum Chem.* **2018**, *119*, e25766.
[39] E. Florez, N. Acelas, F. Ramírez, C. Hadad, A. Restrepo, *Phys. Chem. Chem. Phys.* **2018**, *20*, 8909.
[40] S. Gomez, A. Maldonado, G. Aucar, *J. Chem. Phys.* **2005**, 123, 214108.
[41] A. Maldonado, G. Aucar, *Phys. Chem. Chem. Phys.* **2009**, 11, 5615.
[42] J. Perez, A. Restrepo, *ASCEC V-02: Annealing Simulado Con Energía Cuántica, Property, Development and Implementation*, Grupo de Química Física Teórica, Instituto de Química, Universidad de Antioquia, Medellín, Colombia **2008**.
[43] J. Pérez, C. Hadad, A. Restrepo, *Int. J. Quantum Chem.* **2008**, *108*, 1653.
[44] J. F. Pérez, E. Florez, C. Z. Hadad, P. Fuentealba, A. Restrepo, *J. Phys. Chem. A* **2008**, *112*, 5749.
[45] F. Weigend, R. Ahlrichs, *Phys. Chem. Chem. Phys.* **2005**, *7*, 3297.
[46] D. Rappoport, F. Furche, *J. Chem. Phys.* **2010**, *133*, 134105.

[47] K. A. Peterson, D. Figgen, E. Goll, H. Stoll, M. Dolg, *J. Chem. Phys.* **2003**, *119*, 11113.
[48] M. Frisch, G. Trucks, H. B. Schlegel, G. E. Scuseria, M. A. Robb, J. R. Cheeseman, et al., *Gaussian 09*, *Revision D. 01*, Gaussian, Inc, Wallingford, CT **2009**.
[49] DIRAC, a relativistic ab initio electronic structure program, Release DIRAC17, http://www.diracprogram.org, L. Visscher, H. J. Aa. Jensen, R. Bast, and T. Saue, with contributions from V. Bakken, K. G. Dyall, S. Dubillard, U. Ekström, E. Eliav, T. Enevoldsen, E. Faßhauer, T. Fleig, O. Fossgaard, A. S. P. Gomes, E. D. Hedegård, T. Helgaker, J. Henriksson, M. Iliaš, Ch. R. Jacob, S. Knecht, S. Komorovský, O. Kullie, J. K. Lærdahl, C. V. Larsen, Y. S. Lee, H. S. Nataraj, M. K. Nayak, P. Nor-man, G. Olejniczak, J. Olsen, J. M. H. Olsen, Y. C. Park, J. K. Pedersen, M. Pernpointner, R. di Remigio, K. Ruud, P. Sałek, B. Schimmelpfennig, A. Shee, J. Sikkema, A. J. Thorvaldsen, J. Thyssen, J. van Stralen, S. Villaume, O. Visser, T. Winther, and S. Yamamoto.
[50] A. J. Sadlej, *Collect. Czech. Chem. Commun.* **1988**, *53*, 1995.
[51] A. J. Sadlej, *Theor. Chem. Acc.* **1991**, *81*, 45.
[52] A. J. Sadlej, *Theor. Chem. Acc.* **1992**, *81*, 339.
[53] K. G. Dyall, *Theor. Chem. Acc.* **2006**, *115*, 441.
[54] R. Bader, *Atoms in Molecules: A Quantum Theory*, Oxford University Press, Oxford **1990**.
[55] Keith T. AIMAll version 10.09. 12. TK Gristmill Software, https://www.aim.tkgristmill.com **2010**.
[56] J. Romero, A. Reyes, J. David, A. Restrepo, *Phys. Chem. Chem. Phys.* **2011**, *13*, 15264.
[57] E. Flórez, A. Maldonado, G. Aucar, J. David, A. Restrepo, *Phys. Chem. Chem. Phys.* **2016**, *18*, 1537.
[58] S. Jenkins, A. Restrepo, J. David, D. Yin, S. R. Kirk, *Phys. Chem. Chem. Phys.* **2011**, *13*, 11644.
[59] J. Kim, H. M. Lee, S. B. Suh, D. Majumdar, K. S. Kim, *J. Chem. Phys.* **2000**, *113*, 5259.
[60] S. F. Boys, F. Bernardi, *Mol. Phys.* **1970**, *19*, 553.
[61] P. Botschwina, H. Stoll, *Phys. Chem. Chem. Phys.* **2001**, *3*, 1965.
[62] E. Espinosa, I. Alkorta, J. Elguero, E. Molins, *J. Chem. Phys.* **2002**, *117*, 5529.
[63] N. Acelas, G. Hincapié, D. Guerra, J. David, A. Restrepo, *J. Chem. Phys.* **2013**, *139*, 044310.
[64] K. D. Collins, M. W. Washabaugh, *Q. Rev. Biophys.* **1985**, *18*, 323.
[65] A. Zapata-Escobar, M. Manrique-Moreno, D. Guerra, C. Hadad, A. Restrepo, *J. Chem. Phys.* **2014**, *140*, 05B611_1.
[66] N. Rojas-Valencia, C. Ibargüen, A. Restrepo, *Chem. Phys. Lett.* **2015**, *635*, 301.
[67] F. Ramírez, C. Hadad, D. Guerra, J. David, A. Restrepo, *Chem. Phys. Lett.* **2011**, *507*, 229.
[68] S. J. Grabowski, *Chem. Rev.* **2011**, *111*, 2597.
[69] Pauling L. *The Nature of the Chemical Bond: and the Structure of Molecules and Crystals; an Introduction to Modern Structural Chemistry*, Cornell University Press, Ithaka, New York, **1940**.
[70] C. Coulson, *Valence*, Oxford University Press, London **1961**.

SUPPORTING INFORMATION

Additional supporting information may be found online in the Supporting Information section at the end of this article.

How to cite this article: Chamorro Y, Flórez E, Maldonado A, Aucar G, Restrepo A. Microsolvation of heavy halides. *Int J Quantum Chem*. 2021;121:e26571. https://doi.org/10.1002/qua.26571